

# Supporting Information: Unraveling Disorder-to-Order Transitions and Chemical Ordering in PtCoM Ternary Alloys Using Machine Learning Potential

Xiangfu Niu,<sup>†,‡,¶,§</sup> Shiyu Zhen,<sup>†,‡,¶,§</sup> Rui Zhang,<sup>§</sup> Jianqiu Li,<sup>‡,¶,§</sup> and Liang  
Zhang<sup>\*,†,‡,¶,§</sup>

<sup>†</sup>*Center for Combustion Energy, Tsinghua University, Beijing, 100084, China*

<sup>‡</sup>*School of Vehicle and Mobility, Tsinghua University, Beijing, 100084, China*

<sup>¶</sup>*State Key Laboratory of Intelligent Green Vehicle and Mobility*

<sup>§</sup>*Beijing Huairou Laboratory, Beijing, 101400, China*

E-mail: zhangbright@tsinghua.edu.cn

## DFT Calculations

The dataset used for model training comprises a wide range of Pt<sub>2</sub>CoM bulk systems. It includes previously studied systems such as PtCo, Pt<sub>2</sub>CoCu, Pt<sub>2</sub>CoNi, Pt<sub>2</sub>CoMn, Pt<sub>2</sub>CoFe, Pt<sub>2</sub>CoGa, and Pt<sub>2</sub>CoTi,<sup>1</sup> as well as additional compositions where M = Cr, Zn, Nb, Mo, Ru, Rh, Pd, Ag, Cd, Ta, W, Re, Os, Ir, Pt, Au, and Hg. These elements span diverse groups and periods in the periodic table, significantly enriching the chemical space of the dataset. To ensure adequate coverage of structural complexity, we systematically sampled configurations with varying degrees of M-site ordering, using a hierarchical approach that captures ordering patterns across both Pt–Co/M and Co–M sublattices. To ensure the robustness and generalizability of the developed machine learning potential, we constructed a diverse training dataset that includes not only fully optimized structures at local minima but also non-equilibrium configurations. Specifically, we generated PtCoM alloy structures with varying degrees of ordering and extracted structural, energetic, and force information from each ionic step during their DFT relaxation trajectories. This approach enables the model to learn from configurations that deviate from equilibrium, enhancing its reliability in practical simulations. In addition, the pretrained DPA model was initialized using the OC20 dataset, which contains extensive non-equilibrium data, including DFT trajectories, single-point calculations on randomly perturbed structures, and short-time high-temperature AIMD simulations. These diverse data sources provide rich coverage of the potential energy surface, enabling the model to accurately describe both near-equilibrium and far-from-equilibrium structures.

DFT calculations were carried out using the Vienna Ab Initio Simulation Package (VASP).<sup>2</sup> The core and valence electron interactions were modeled using the projected-augmented wave (PAW) method.<sup>3</sup> A plane-wave basis set with a kinetic energy cutoff of 400 eV was applied. The exchange-correlation energy was approximated using the Perdew-Burke-Ernzerhof (PBE) functional within the generalized gradient approximation (GGA).<sup>4</sup> An energy convergence criterion of  $5 \times 10^{-5}$  eV was set for electronic structure calculations, and the geometry

optimization was performed until the forces on all atoms were below 0.03 eV/Å. The PtCo unit cell, with the P4/mmm space group, was obtained from the Materials Project.<sup>5</sup> To create the Pt<sub>2</sub>CoM unit cell (where M represents the third element doped into PtCo), the PtCo unit cell was replicated, and one of the Co atoms was replaced by an M atom. The lattice constants of the Pt<sub>2</sub>CoM unit cells were then re-optimized using DFT. A (3×3×3) supercell was constructed based on the DFT-optimized Pt<sub>2</sub>CoM unit cell, which contains a total of 108 atoms. The (3×3×3) and (9×9×9) Monkhorst-Pack k-point grids were utilized to sample the Brillouin zone for the unit cell and supercell model.<sup>6</sup>

## Monte Carlo Simulation

The Monte Carlo process employed in this study aims to explore atomic configurations and calculate various thermodynamic properties, including short-range order (SRO), free energy, and configurational entropy, for a system composed of three atomic species (Pt, Co, M). A fixed cutoff radius of 1.4 Å is used to define the neighbors for each atom, and this neighbor list is then utilized to compute the short-range order (SRO), which is tracked throughout the simulation to monitor the system’s local ordering behavior. The potential energy for each configuration is evaluated using a fine-tuned machine learning potential model, and the configuration is optimized via the BFGS algorithm to minimize atomic forces. Configurational entropy is subsequently calculated by considering the distribution of atomic types and the probabilities of different pairwise configurations in the neighbor list. The formula for calculating configurational entropy is:

$$S_{mix} = k_B \sum_{j,k=1}^n c_j f_{jk} \ln \left( \frac{\sum_{l=1}^n c_l f_{lk}}{c_j f_{jk}} \right) \quad (1)$$

where  $c_j$  is the ratio of element  $j$ ,  $k_B$  is the Boltzmann constant, and  $f_{ij}$  is the probability of finding a  $j$  atom next to a  $k$  atom. The Monte Carlo simulation iteratively generates new atomic configurations by randomly swapping atom types between neighboring atoms. The

Metropolis criterion is applied to accept or reject mutated configurations based on changes in free energy. If the energy decreases, the new configuration is always accepted; otherwise, it is accepted with a probability proportional to the Boltzmann factor. Key thermodynamic properties, including energy, SRO, enthalpy, and entropy, are recorded at each Monte Carlo step. The final configuration with the lowest energy is saved, along with data on SRO and free energy. The simulation consists of 5000 steps and is independently repeated five times to select the configuration with the minimum energy, thereby avoiding local minima.

### Ordering energy calculation

To calculate the thermodynamic driving force for the disorder-to-order in PtCo and Pt<sub>2</sub>CoM systems, we randomly generated Pt<sub>2</sub>CoM configurations with predefined degrees of ordering. Monte Carlo algorithm was applied to swap atomic positions such that the structural ordering evolved toward the target value. The finetuned machine learning potential was then used to optimize these structures and evaluate their energies. For PtCo, one ordered structure with  $\alpha^{\text{Pt-Co}} = -1/3$  and 180 random structures with  $\alpha^{\text{Pt-Co}} = 0$  were generated. For Pt<sub>2</sub>CoM, we generated 180 ordered structures with  $\alpha^{\text{Pt-Co/M}} = -1/3$ , which exhibit varying degrees of Co-M ordering ( $\alpha^{\text{Co-M}} = -6/54, 1/54, 8/54, 15/54, 22/54, 29/54, 36/54, 43/54, 50/54$ ), as well as 180 random structures with  $\alpha^{\text{Pt-Co/M}} = 0$ .

### Estimation of Bond Energies for Co-M, M-M, and Co-Co Pairs

To approximate the relative bond strengths of Co-M, M-M, and Co-Co pairs discussed, we employed a simplified bond decomposition approach based on total energies of representative supercell structures. Specifically, we constructed bulk models of pure Pt, Co, and M metals, as well as ordered ternary PtCoM alloys and related binary systems including PtCo and PtM. The supercell contains 108 atoms, each coordinated with 12 nearest neighbors. Considering each pair is counted once, this results in 648 unique nearest-neighbor bonds. We then assumed that the total energy of each structure can be approximately decomposed into

contributions from these 648 pairwise bonds, following the relations:

$$E_{\text{Pt bulk}} = 648 E_{\text{Pt-Pt}} \quad (2)$$

$$E_{\text{Co bulk}} = 648 E_{\text{Co-Co}} \quad (3)$$

$$E_{\text{M bulk}} = 648 E_{\text{M-M}} \quad (4)$$

$$E_{\text{PtCo bulk}} = 108 E_{\text{Pt-Pt}} + 108 E_{\text{Co-Co}} + 432 E_{\text{Pt-Co}} \quad (5)$$

$$E_{\text{PtM bulk}} = 108 E_{\text{Pt-Pt}} + 108 E_{\text{M-M}} + 432 E_{\text{Pt-M}} \quad (6)$$

$$E_{\text{PtCoM bulk}} = 108 E_{\text{Pt-Pt}} + 9 E_{\text{Co-Co}} + 9 E_{\text{M-M}} + 216 E_{\text{Pt-Co}} + 216 E_{\text{Pt-M}} + 90 E_{\text{Co-M}} \quad (7)$$

Solving this system of six linear equations yields approximate values for the six bond energies: Pt-Pt, Co-Co, M-M, Pt-Co, Pt-M, and Co-M. This pairwise decomposition is a simplification that neglects many-body effects and local environmental variations, but it serves as a reasonable approximation to assess the relative bond preferences. These estimates were used to rationalize the energetic driving forces behind elemental ordering or segregation in PtCoM ternary alloys, as illustrated in Figure S7.

## Vacancy Migration Energy Barrier Calculation

We fine-tuned the machine learning potential by incorporating a small set of transition-state data from climbing image nudged elastic band (CI-NEB) calculations of vacancy migration in PtCo, aiming to improve its accuracy in predicting transition states. Then the model was used to calculate the vacancy migration energy barrier in PtCoM. The vacancy is introduced by randomly removing a metal atom from the PtCoM system. The structures before and after the vacancy migration are optimized using a machine learning potential, which serves as the initial and final configurations for the transition state calculation. To represent the reaction pathway, intermediate structures—referred to as NEB images—are created between the initial and final states. In this study, three intermediate images are generated, resulting

in a total of five images: one initial, three intermediate, and one final. The atomic positions of these intermediate images are interpolated to generate an initial reaction path connecting the initial and final configurations. The machine learning potential model is then used to calculate the forces acting on the atoms and the potential energy of the system, ensuring accurate energy calculations during the optimization process. The NEB path is subsequently optimized using the BFGS algorithm, which iteratively minimizes the forces on the atoms. The optimization continues until a force tolerance of  $0.03 \text{ eV}/\text{\AA}$  is achieved. This optimized path provides the basis for determining the transition state energy and activation barrier for the vacancy migration process.

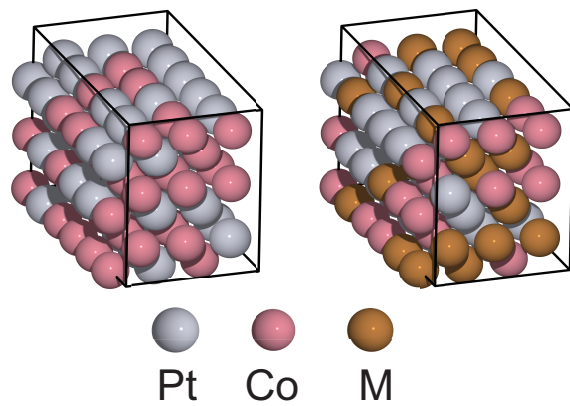


Figure 1: The PtCo and PtCoM supercell model containing 108 atoms.

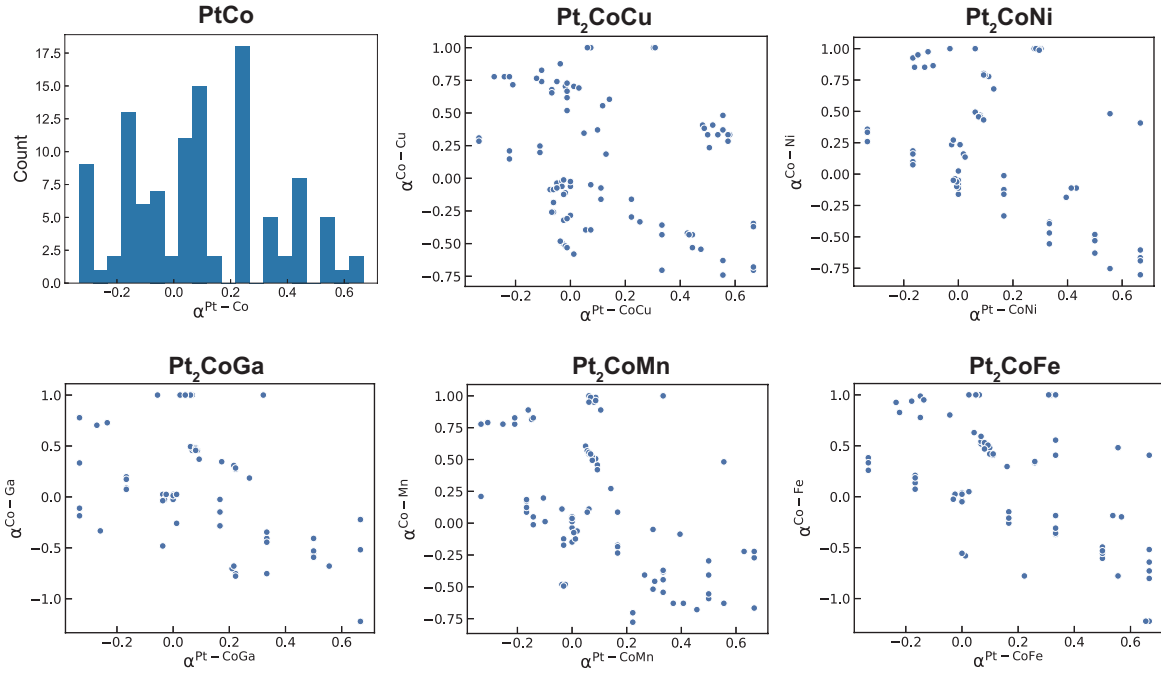


Figure 2: Distribution of ordering degree for PtCo, Pt<sub>2</sub>CoCu, Pt<sub>2</sub>CoNi, Pt<sub>2</sub>CoGa, Pt<sub>2</sub>CoMn and Pt<sub>2</sub>CoFe dataset.

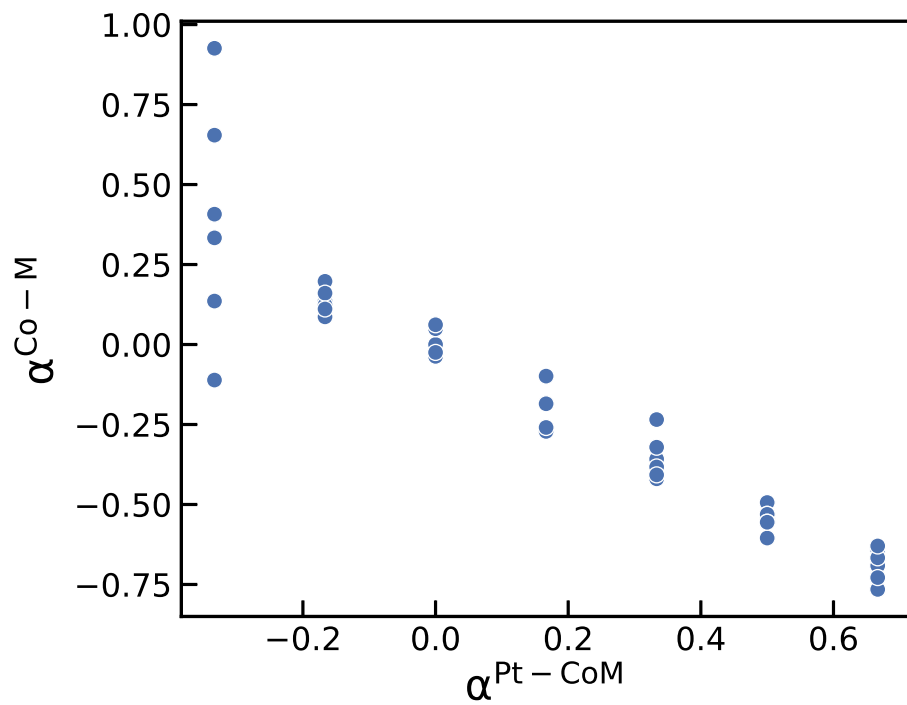


Figure 3: Distribution of ordering degree for  $\text{Pt}_2\text{CoM}$  dataset ( $M=\text{Cr, Zn, Nb, Mo, Ru, Rh, Pd, Ag, Cd, Ta, W, Re, Os, Ir, Pt, Au, Hg}$ ).

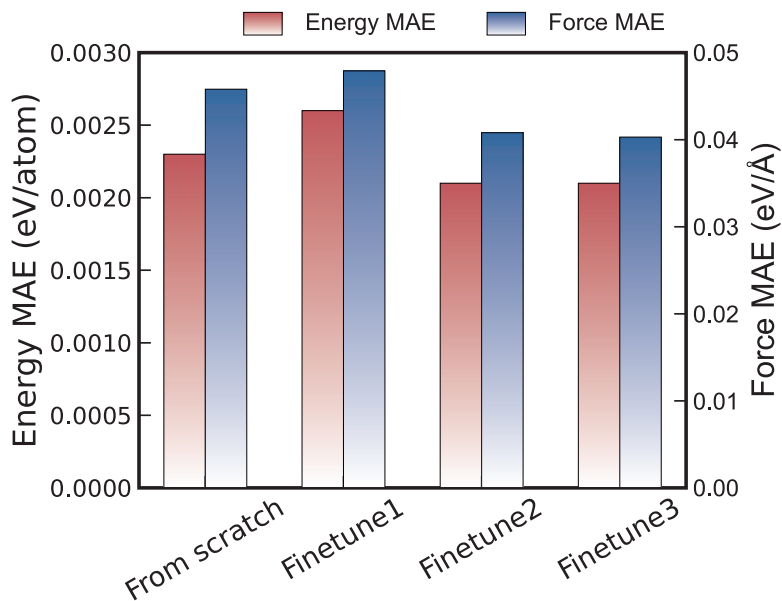


Figure 4: Comparison of different fine-tuning strategies: "From scratch" refers to training a model from the beginning, where all parameters are re-initialized without inheriting any from a pre-trained model; "Finetune1" adjusts only the parameters in the fitting network, while keeping all other parameters frozen; "Finetune2" allows adjustment of both the fitting and descriptor network parameters; "Finetune3" allows all parameters to be adjusted.

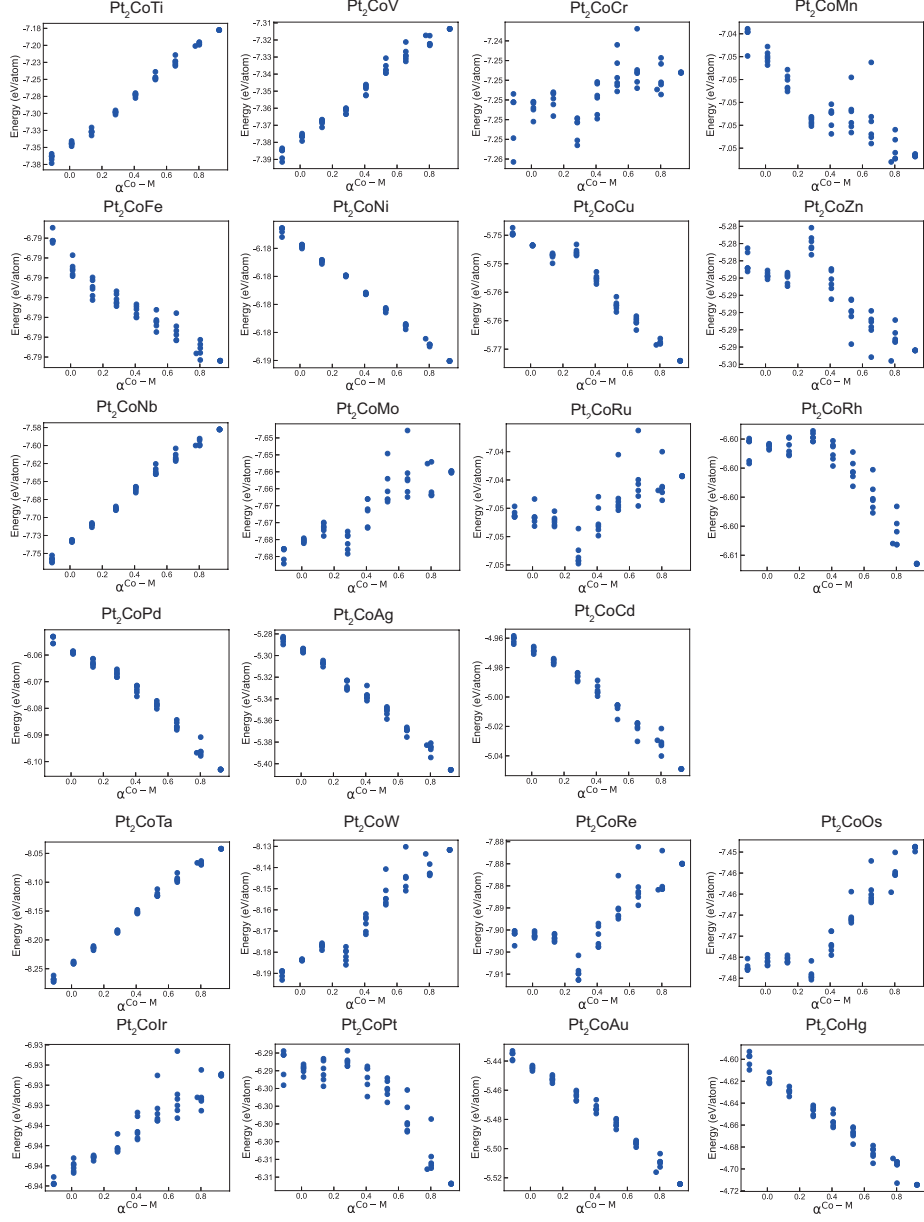


Figure 5: Machine learning predicted energy as a function of  $\alpha^{\text{Co-M}}$  at  $\alpha^{\text{Pt-CoM}}=-1/3$  for different kinds of  $\text{Pt}_2\text{CoM}$ .

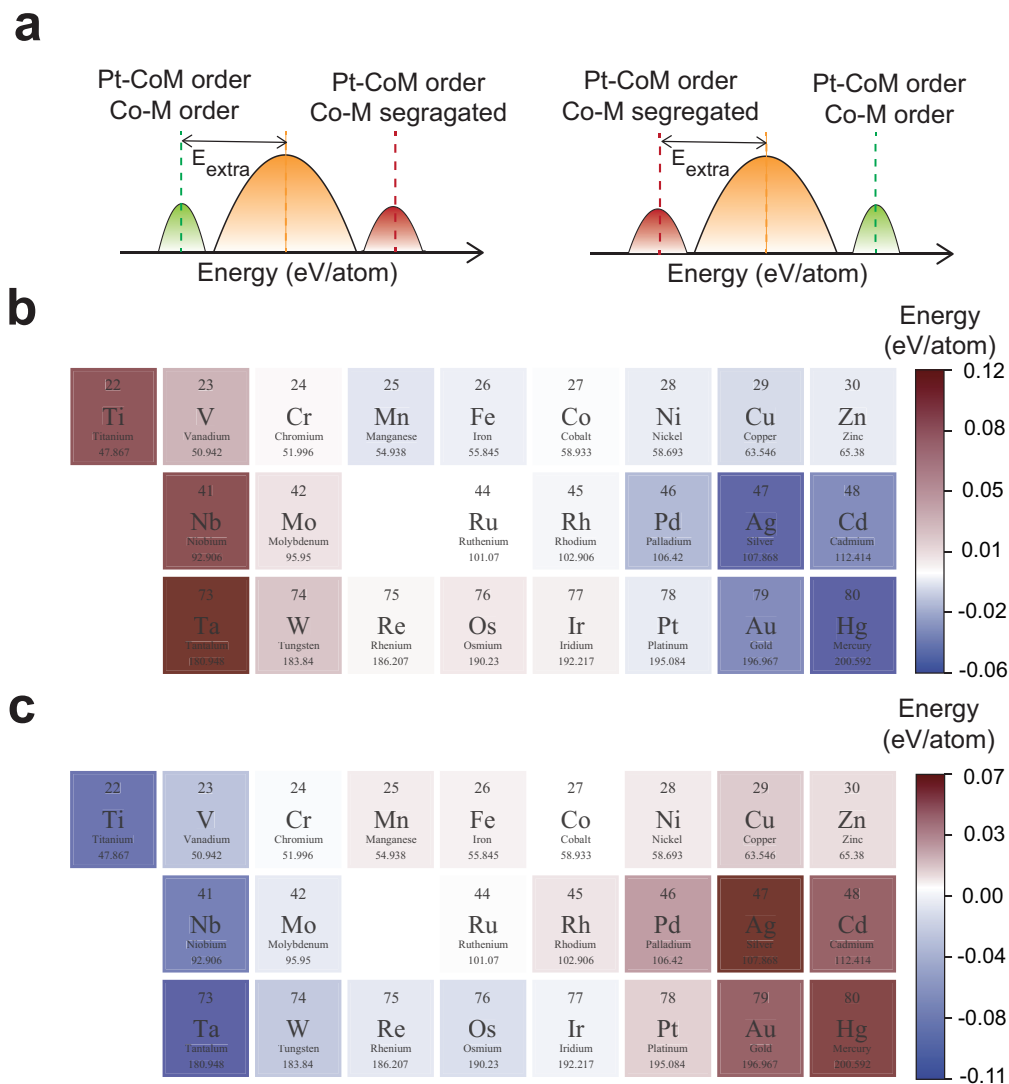


Figure 6: (a) Depiction of mean energy difference between structures with diverse chemical  $\alpha^{\text{Co-M}}$  at  $\alpha^{\text{Pt-CoM}} = -1/3$ . (b) Energy differences between ordered ( $\alpha^{\text{Co-M}} = -3/27$ ) and randomly arranged Co and M atom structures. (c) Energy differences between segregated ( $\alpha^{\text{Co-M}} = 25/27$ ) and randomly arranged Co and M atom structures.

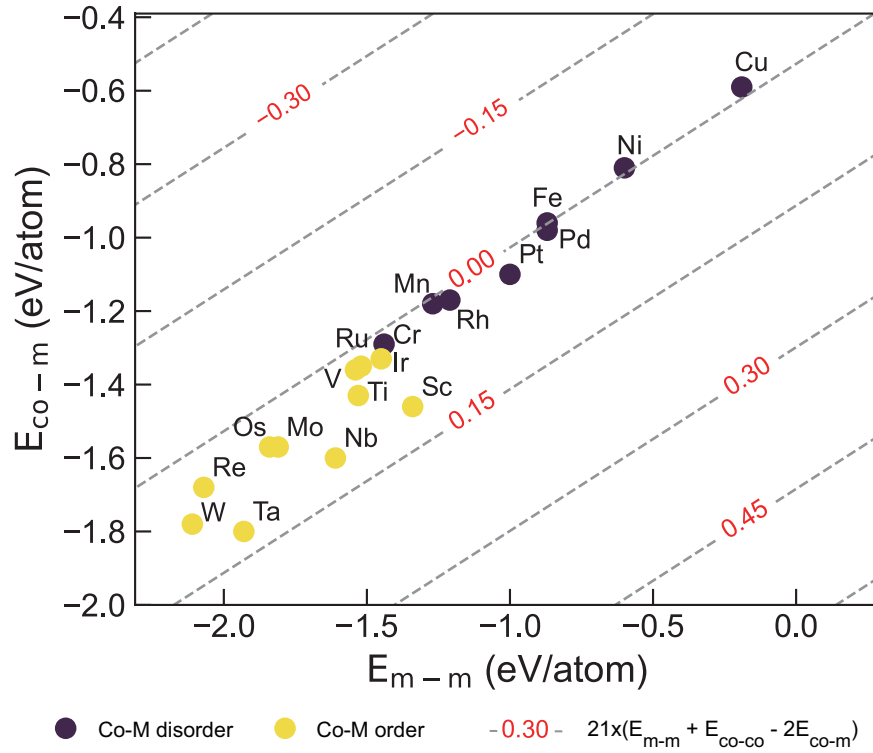


Figure 7: Distribution of elements tend to disorder or order as a function of  $E_{\text{Co-M}}$  and  $E_{\text{M-M}}$ .

Table 1: The number of DFT calculated configurations for different  $\text{Pt}_2\text{CoM}$  used to training machine learning potential.

Alloy	Number	Alloy	Number
$\text{PtCo}$	109	$\text{Pt}_2\text{CoRh}$	35
$\text{Pt}_2\text{CoCu}$	120	$\text{Pt}_2\text{CoPd}$	35
$\text{Pt}_2\text{CoNi}$	116	$\text{Pt}_2\text{CoAg}$	35
$\text{Pt}_2\text{CoGa}$	107	$\text{Pt}_2\text{CoCd}$	35
$\text{Pt}_2\text{CoMn}$	106	$\text{Pt}_2\text{CoTa}$	35
$\text{Pt}_2\text{CoFe}$	116	$\text{Pt}_2\text{CoW}$	35
$\text{Pt}_2\text{CoTi}$	116	$\text{Pt}_2\text{CoRe}$	35
$\text{Pt}_2\text{CoV}$	35	$\text{Pt}_2\text{CoOs}$	35
$\text{Pt}_2\text{CoCr}$	35	$\text{Pt}_2\text{CoIr}$	35
$\text{Pt}_2\text{CoZn}$	35	$\text{Pt}_2\text{CoPt}$	35
$\text{Pt}_2\text{CoNb}$	35	$\text{Pt}_2\text{CoAu}$	35
$\text{Pt}_2\text{CoMo}$	35	$\text{Pt}_2\text{CoHg}$	35
$\text{Pt}_2\text{CoRu}$	35		

Table 2: Thermodynamic driving force for PtCoCu ordering under different sampling numbers

Sampling number	Thermodynamic driving force (eV/atom)
9	0.0824
27	0.0828
35	0.0829
135	0.0825
180	0.0821
270	0.0817
360	0.0816
405	0.0817

Table 3: Comparison of energy prediction accuracy for different machine learning modeling approaches on PtCo-based ternary alloys

Model	Dataset	Energy MAE (eV/atom)
Finetuned DPA	PtCoM	0.0022
Finetuned MACE	PtCoM	0.0029
Cluster Expansion	PtCoCu	0.0082
	PtCoNi	0.0035
Descriptor + GPR	PtCoCu	0.0058
	PtCoNi	0.0036

Table 4: Experimental synthesis cases of highly ordered Pt<sub>2</sub>CoM alloys for ORR electrocatalyst.

<b>Alloy</b>	<b>Reference</b>
PtCoTi	<i>ACS Catalysis</i> , <b>2022</b> , 12(13): 7571–7578
PtCoV	<i>Chemistry of Materials</i> , <b>2012</b> , 24(22): 4283–4293
PtCoNi	<i>Nature Communications</i> , <b>2024</b> , 15(1): 415 <i>JACS</i> , <b>2020</b> , 142(45): 19209–19216 <i>Nano Energy</i> , <b>2024</b> , 120: 109154
PtCoCu	<i>Nature Communications</i> , <b>2024</b> , 15(1): 415 <i>JACS</i> , <b>2020</b> , 142(45): 19209–19216
PtCoZn	<i>Journal of Colloid and Interface Science</i> , <b>2023</b> , 652: 388–404
PtCoAg	<i>Electrochimica Acta</i> , <b>2016</b> , 219: 531–539
PtCoAu	<i>Electrochimica Acta</i> , <b>2021</b> , 384: 138266 <i>Advanced Functional Materials</i> , <b>2020</b> , 30(22): 2001575

Table 5: Machine learning predicted average energy difference between the ordered arrangement of Pt and Co/M structures ( $\alpha^{\text{Pt-CoM}} = -1/3$ ) and the random arrangement of Pt and Co/M structures ( $\alpha^{\text{Pt-CoM}} = 0$ ).

<b>Metal</b>	<b>Energy difference (eV/atom)</b>	<b>Energy difference relative to PtCo (eV/atom)</b>
Ti	0.0645	0.0028
V	0.0603	-0.0014
Cr	0.0311	-0.0306
Mn	0.0199	-0.0418
Fe	0.0340	-0.0277
Co	0.0617	0.0000
Ni	0.0683	0.0066
Cu	0.0694	0.0077
Zn	0.0894	0.0277
Nb	0.0530	-0.0087
Mo	0.0384	-0.0233
Ru	-0.0091	-0.0708
Rh	0.0224	-0.0393
Pd	0.0362	-0.0255
Ag	0.0407	-0.0210
Cd	0.0686	0.0069
Ta	0.0453	-0.0164
W	0.0250	-0.0367
Re	-0.0266	-0.0883
Os	-0.0485	-0.1102
Ir	-0.0156	-0.0773
Pt	0.0145	-0.0472
Au	0.0263	-0.0354
Hg	0.0383	-0.0234
<b>Max</b>	0.0894	0.0277
<b>Min</b>	-0.0485	-0.1102

Table 6: Machine learning predicted extra ordering energy casued by ordering of Co and M (second column) and segregation of Co and M (third column).

<b>Metal</b>	<b>Energy different (eV/atom)</b>	<b>Energy different (eV/atom)</b>
Ti	0.0921	-0.0930
V	0.0377	-0.0352
Cr	0.0031	-0.0031
Mn	-0.0059	0.0039
Fe	-0.0035	0.0026
Co	0.0000	0.0000
Ni	-0.0045	0.0046
Cu	-0.0097	0.0123
Zn	-0.0051	0.0077
Nb	0.0952	-0.0846
Mo	0.0127	-0.0118
Ru	0.0004	-0.0022
Rh	-0.0018	0.0055
Pd	-0.0209	0.0264
Ag	-0.0544	0.0635
Cd	-0.0380	0.0473
Ta	0.1159	-0.1092
W	0.0273	-0.0310
Re	0.0041	-0.0121
Os	0.0097	-0.0180
Ir	0.0066	-0.0064
Pt	-0.0046	0.0111
Au	-0.0385	0.0469
Hg	-0.0563	0.0554
<b>Max</b>	0.1159	0.0635
<b>Min</b>	-0.0563	-0.1092

Table 7: Mean vacancy diffusion barrier in PtCo, PtCoCu, PtCoNi, and PtCoZn.

System	Atom	Mean vacancy diffusion barrier (eV/atom)
PtCo	Pt / Co	1.33 / 1.17
PtCoCu	Pt / Co / Cu	1.07 / 1.02 / 0.76
PtCoNi	Pt / Co / Ni	1.06 / 1.06 / 0.97
PtCoZn	Pt / Co / Zn	0.95 / 1.01 / 0.68

## References

- (1) Yin, P.; Niu, X.; Li, S.-B.; Chen, K.; Zhang, X.; Zuo, M.; Zhang, L.; Liang, H.-W. Machine-learning-accelerated design of high-performance platinum intermetallic nanoparticle fuel cell catalysts. Nature Communications **2024**, 15, 415.
- (2) Kresse, G.; Furthmüller, J. Efficient iterative schemes for ab initio total-energy calculations using a plane-wave basis set. Physical Review B **1996**, 54, 11169.
- (3) Kresse, G.; Joubert, D. From ultrasoft pseudopotentials to the projector augmented-wave method. Physical Review B **1999**, 59, 1758.
- (4) Perdew, J. P.; Burke, K.; Ernzerhof, M. Generalized gradient approximation made simple. Physical Review Letters **1996**, 77, 3865.
- (5) Jain, A.; Ong, S. P.; Hautier, G.; Chen, W.; Richards, W. D.; Dacek, S.; Cholia, S.; Gunter, D.; Skinner, D.; Ceder, G.; others Commentary: The Materials Project: A materials genome approach to accelerating materials innovation. APL Materials **2013**, 1.
- (6) Monkhorst, H. J.; Pack, J. D. Special points for Brillouin-zone integrations. Physical Review B **1976**, 13, 5188.